RSC Medicinal Chemistry

ROYAL SOCIETY OF CHEMISTRY

RESEARCH ARTICLE

View Article Online
View Journal

Cite this: DOI: 10.1039/d6md00211k

Identification and structure–activity relationship analysis of minimal fusion inhibitors targeting measles virus F protein

Kazuya Kobayashi, [a] Yuki Yamaguchi,[a] Mizuki Itahara,[a] Kazushige Hirata, [b] Keisuke Aoki,[ac] Naoya Iwamoto, [a] Hironori Hayashi, [d] Eiichi Kodama [de] and Shinya Oishi *[a]

Although measles has been effectively controlled by vaccination, sporadic outbreaks still occur worldwide, highlighting the need for antiviral agents as complementary measures to achieve sustained elimination. Previously, we reported an anti-measles virus (MV) peptide derived from the HR2 region of MV fusion (F) protein that inhibits viral membrane fusion by disrupting the interaction between HR1 and HR2 regions. Here, we aimed to optimize this peptide by minimizing its sequence and interaction characteristics, thereby identifying a short derivative that retains potent antiviral activity. Structure–activity relationship analyses revealed that both hydrophobic and polar residues in HR2-derived peptides are crucial for efficient interaction with HR1. Thermal stability analysis of potential six-helical bundles using HR1-40, a 40-residue peptide of the HR1 region, showed no clear correlation with antiviral activity. To address this, we designed HR1Y, a C-terminally extended HR1 variant, which allowed a more accurate assessment of complex stability. Furthermore, molecular modeling of the HR2-derived peptide–HR1Y complex reproduced several experimental trends and provided structural insight into the HR1–HR2 interface. These findings clarify the structural determinants of fusion inhibitors against MV and support the rational optimization of HR2-derived antiviral peptides.

Received 16th March 2026,
Accepted 2nd May 2026

DOI: 10.1039/d6md00211k

rsc.li/medchem

Introduction

Measles is a highly contagious and pathogenic infectious disease caused by the measles virus (MV), a member of the genus *Morbillivirus* within the family *Paramyxoviridae*.[1] The main symptoms include fever, cough, coryza, conjunctivitis, and maculopapular rash.[2,3] Severe complications such as pneumonia and encephalitis may occur, and in some cases, the disease can be fatal. Although vaccination has been widely implemented as a preventive measure against measles,[4] sporadic infections still occur in unvaccinated infants and in cases involving imported viruses.[5] Moreover, it has been reported that years to decades after infection and recovery, some patients may develop subacute sclerosing panencephalitis (SSPE), emphasizing the need for effective antiviral drugs against MV.[6]

MV is an enveloped virus surrounded by a lipid bilayer. The envelope contains two glycoproteins, hemagglutinin (H) and fusion (F) proteins. During viral entry, the H protein first binds to host cell receptors, followed by conformational changes in the F protein.[7,8] Specifically, the HR1 region of the F protein forms a three-helix bundle, and the exposed fusion peptide (FP) inserts into the host cell membrane. Subsequently, the HR2 regions rearrange to bind the surface of the three-helix bundle, forming a six-helix bundle that brings the host and viral membranes into proximity, leading to membrane fusion.[9]

The entry of some class I enveloped viruses relies on the interaction between HR1 and HR2 domains of their fusion proteins. Therefore, disruption of this interaction can block membrane fusion. Synthetic peptides designed from the HR2 sequence exploit this mechanism by binding competitively to the viral HR1 trimer as potent decoys, thereby preventing HR2 from associating and exerting antiviral effects.[10–12] Therefore, several HR2-derived peptides from the measles virus F protein have been reported to inhibit viral replication.[13–17] Other classes of measles virus fusion

[a] *Laboratory of Medicinal Chemistry, Kyoto Pharmaceutical University, Yamashina-ku, Kyoto 607-8412, Japan. E-mail: soishi@mb.kyoto-phu.ac.jp; Tel: +81 75 595 4635*
[b] *Department of Clinical Laboratory Medicine, Tohoku University Hospital, Sendai 980-8574, Japan*
[c] *Graduate School of Pharmaceutical Sciences, Kyoto University, Kyoto 606-8501, Japan*
[d] *Division of Infectious Diseases, International Research Institute of Disaster Science, Tohoku University, Sendai 980-8575, Japan*
[e] *Department of Infectious Diseases, Graduate School of Medicine and Tohoku Medical Megabank Organization, Tohoku University, Sendai 980-8575, Japan*

inhibitors have also been reported, including fusion inhibitor peptides (FIP)[18] and neutralizing antibodies targeting the F protein.[19] These inhibitors act through distinct mechanisms by interfering with conformational changes of the F protein.[20,21] Previously, we identified an HR2-derived peptide, M1 (**1**; Fig. 1A), which could inhibit MV replication, including that of viral variants, under *in vitro* conditions.[15] To enhance the antiviral activity, we designed a derivative, M1EK (**2**), by introducing α-helix-inducing X-EE-XX-KK motifs into **1**,[15] which could improve the peptide solubility and stabilize the α-helical structure by promoting intramolecular salt bridge formation. To achieve this, solvent-exposed residues (b, c, f, g) were systematically substituted with glutamic acid and lysine, whereas key interaction residues (a, d, e) were preserved (Fig. 1B).[22–24] However, peptide **2** was significantly less potent than peptide **1**, despite the improved α-helicity. This lack of potency may be due to unfavorable conformational changes induced by systematic substitutions that disrupt the essential interactions with HR1 trimer. To address this, we optimized the introduction sites of the X-EE-XX-KK motifs based on the X-ray crystal structure of the **1**–HR1-42 peptide complex (Fig. 1C), leading to the identification of MEK35GT (**3**), which showed more potent antiviral activity.[25]

In the present work, based on the sequence of **3**, we conducted structure–activity relationship (SAR) studies, in which a series of short fusion-inhibitory peptides was designed and synthesized. The secondary structure and thermal stability of the derivatives in the presence of an HR1-derived peptide were investigated by circular dichroism (CD) spectroscopy. We also assessed the applicability of HR1-derived peptides with C-terminally extended sequences by comparing CD spectra to rationalize the structure–activity relationship of HR2 derivatives, focusing on the secondary structure and thermal stability of a potential six-helical bundle. Furthermore, we constructed molecular models of six-helix bundles formed by HR2 derivatives and the optimized HR1 peptide, and used these models to gain further insights into the SAR.

Results and discussion

Optimization of the sequence length of the HR2-derived peptides

C-terminal region of the HR2-derived peptide. Starting from MEK35GT (**3**), we aimed to identify shorter sequences for fusion inhibitors that maintain antiviral activity. To this end, we designed three derivatives [MEK28GT (**4**), MEK21GT (**5**), and MEK14GT (**6**)], each with successive 7-residue truncations from the C-terminus of **3**. The peptides were synthesized using a standard Fmoc-based solid-phase synthesis protocol. The antiviral activities were evaluated by measuring inhibition of infection with the human HV Edmonton strain in B95a cells using a 3-(4,5-dimethylthiazol-2-yl)-2,5-diphenyltetrazolium bromide (MTT) cell viability assay. Peptide **4** exhibited high antiviral activity, equipotent with the original peptide M1 (**1**), but was 4-fold less potent than **3** [EC_{50} (**4**) = 0.0092 μM] (Table 1). By contrast, the antiviral activities of **5** and **6** were markedly diminished [EC_{50} (**5**) >10 μM; EC_{50} (**6**) >10 μM]. These results suggest that truncation of the C-terminal seven residues in **3** slightly affects the antiviral activity, whereas further truncation results in a loss of activity. We also evaluated the antiviral activities of peptides **3** and **4** against three MV variants ($MeV_{M1}{}^{R}{}_{p29}$, $MeV_{M1}{}^{R}{}_{p62}$, and $MeV_{M2}{}^{R}{}_{p44}$) generated by induction of drug resistance *in vitro*.[26] Peptide **3** retained antiviral activity against these resistant variants, while a significant reduction in antiviral activity was observed for

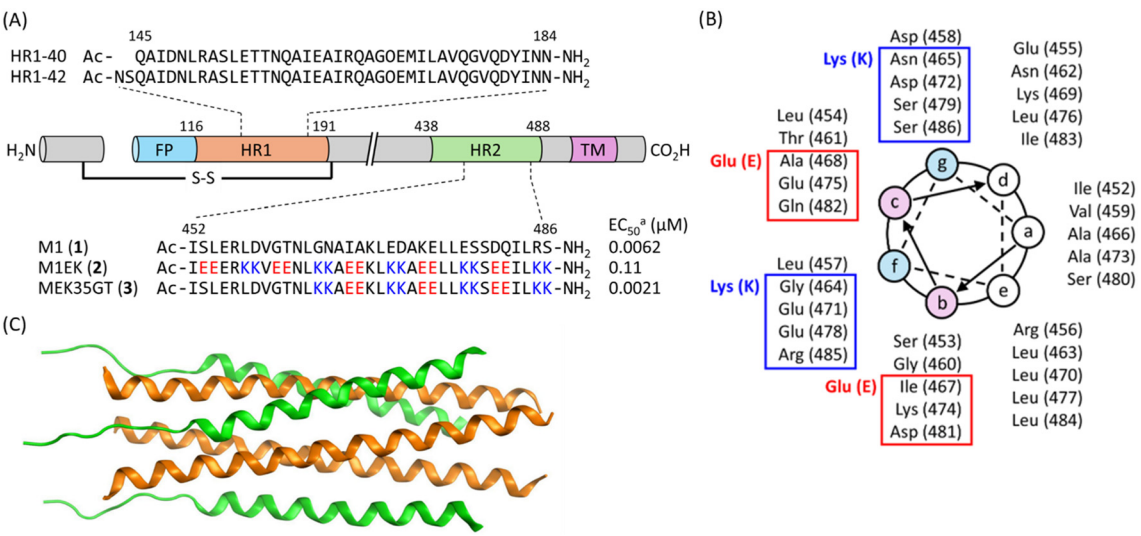

Fig. 1 Structures of MV F protein and its peptide derivatives. (A) Schematic representation of the MV F protein and the sequences of helical repeats. FP: Fusion peptide; HR: heptad repeat; TM: transmembrane domain; S–S: disulfide bond linkage. [a]EC_{50} is the concentration required to inhibit viral replication by 50% in the B95a cells.[25] (B) Helical-wheel representation of M1 (**1**) and their systematic modifications with Glu and Lys for MEK35GT (**3**). (C) Crystal structure of M1 (**1**, green) and HR1-42 (orange) complex (PDB ID:8XNE).

Table 1 Antiviral activity and CD analysis of M1 (**1**) and derivatives **2**–**6**

Peptide	Sequence	EC_{50}[a] (μM) [pEC_{50} ± SD]		CD analysis	
				$[\theta]_{222}$[b]	T_m[c] (°C)
M1 (**1**)	Ac-ISLERLDVGTNLGNAIAKLEDAKELLESSDQILRS-NH_2	0.0062[d]	[8.2 ± 0.4][d]	−18 251[d]	58.2[d]
M1EK (**2**)	Ac-IEEERKKVEENLKKAEEKLKKAEELLKKSEEILKK-NH_2	0.11[d]	[7.0 ± 0.6][d]	−23 250[d]	68.4[d]
MEK35GT (**3**)	Ac-ISLERLDVGTNLKKAEEKLKKAEELLKKSEEILKK-NH_2	0.0021	[8.7 ± 0.3]	−31 493	85.6
MEK28GT (**4**)	Ac-ISLERLDVGTNLKKAEEKLKKAEELLKK-NH_2	0.0092	[8.0 ± 0.3]	−25 317	43.9
MEK21GT (**5**)	Ac-ISLERLDVGTNLKKAEEKLKK-NH_2	>10		−18 613	28.3
MEK14GT (**6**)	Ac-ISLERLDVGTNLKK-NH_2	>10		−13 196	25.9

[a] The concentration required to inhibit viral replication by 50%. [b] Molar ellipticity at 222 nm of the six-helical bundles formed by the HR2-derived peptides in the presence of equimolar HR1-40. [c] T_m values are defined by the temperature at which half of the peptides are folded, and the other are unfolded. [d] The data obtained in the previous study are shown.[25]

peptide **4** (Table S1). In our previous study, we demonstrated that the residues in the N-terminal non-helical region of the HR2-derived peptide are indispensable to antiviral activity against these resistant variants.[26] The present results further indicated that the C-terminal seven residues in peptide **3** also make a critical contribution to the interaction with viral HR1 bearing resistance-associated mutation(s). These findings suggest that a sufficient number of interactions in peptide **3** are required to offset the decreased interaction(s) arising from such mutations, although the detailed mechanism remains unclear.

We evaluated the secondary structure and thermal stability of complexes formed between the synthetic fusion inhibitors and an HR1-derived peptide using CD spectroscopy. CD spectroscopy was used as a comparative indicator of α-helicity and thermal stability. Each fusion inhibitor was mixed with equimolar amounts of HR1-40,[27] corresponding to HR1 Gln145-Asn184 of the F protein, to form the complex. The CD spectra of peptides **3**–**6** in the presence of HR1-40 exhibited negative CD absorption at 208 nm and 222 nm, which are characteristic features of α-helical structures (Fig. 2A). The molar ellipticity at 222 nm ($[\theta]_{222}$) was used as an indicator of α-helicity for each mixture (Table 1). To evaluate the thermal stability of the resulting α-helical structures, temperature-dependent changes in $[\theta]_{222}$ were monitored to calculate the melting temperature (T_m), defined as the temperature at which 50% of the peptide is denatured (Table 1 and Fig. 2B). Thermal denaturation data were initially analyzed using a two-state fitting model. While this model adequately described some datasets, others exhibited broad transitions, poor fitting, incomplete unfolding within the measured temperature range, or ambiguous baseline regions, in which clear low- or high-temperature plateaus could not be identified, indicating that a two-state model could not adequately describe all datasets. To enable consistent comparison of datasets exhibiting single but non-ideal transitions, apparent T_m values were determined independently of the model by linear regression of the central portion of the normalized transition. This approach was applied only to datasets showing a single, monotonic transition, whereas datasets exhibiting clear multiphasic transitions or incomplete unfolding were excluded from T_m determination. The **5**/HR1-40 and **6**/HR1-40 complexes exhibited less negative $[\theta]_{222}$ and lower T_m values than those of **3** and **4**. The decrease in α-helicity of these short peptides may be attributable to the smaller number of α-helix-inducing motifs in their sequences. The lower T_m values suggest that shortening of the peptide chain may adversely affect the stability of the potential six-helical bundle. Both peptides **5** and **6**, which showed no antiviral activity at 10 μM, exhibited substantially lower T_m values, indicating that antiviral activities and six-helical bundle stability were well correlated.

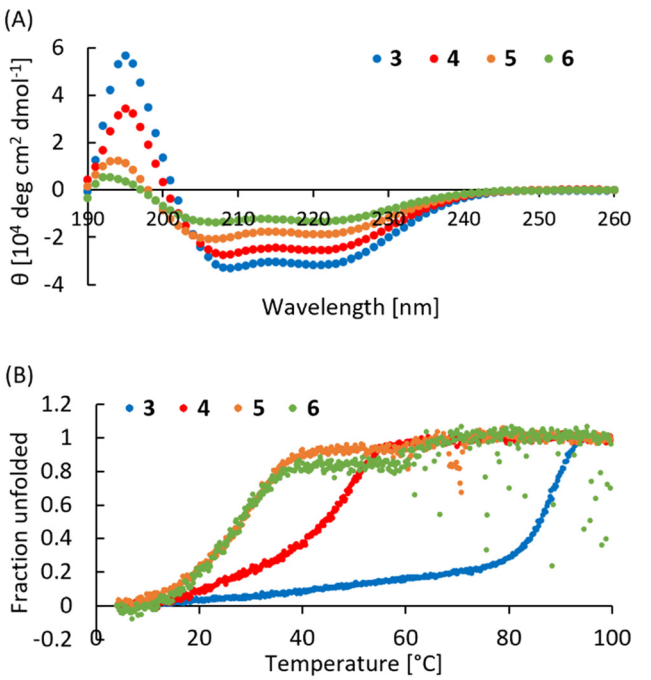

Fig. 2 CD analysis of peptides **3**–**6** in the presence of the HR1-40. (A) CD spectra. (B) Thermal stability of the six-helical bundles.

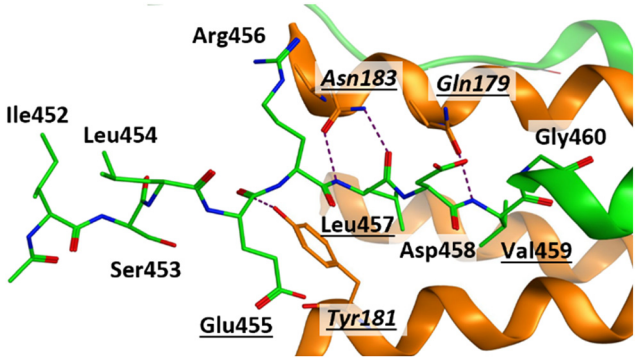

Fig. 3 Interactions between the N-terminal region of **1** (green) and the HR1-42 trimer (orange) (PDB ID: 8XNE). Residues forming hydrogen bonds are underlined, and the residues of HR1-42 are shown in italics.

Collectively, these findings suggest that peptide **4**, with 28 residues, constitutes the minimal sequence required for antiviral activity. Although truncation of the C-terminal sequence in **3** led to a gradual decrease in antiviral activity, peptide **4** retained nanomolar activity and thus represents a valuable lead for further structure–activity relationship studies.

N-terminal region of the HR2-derived peptide. In the X-ray crystal structure of peptide **1**–HR1-42 complex, the N-terminal region (Ile452-Val459) of **1** adopted non-helical structures, and the main chains of Glu455, Leu457, and Val459 formed hydrogen bonds with the HR1 peptide (Fig. 3).[25] Initially, to identify the amino acid residues in the N-terminal non-helical region of **4** that are essential for interaction with the HR1 trimer, we designed and synthesized eight derivatives of **4**, each lacking one residue sequentially from the N-terminus. Sequential truncation from the N-terminus resulted in a gradual decrease in antiviral activity (Table 2). Deletion of the N-terminal Ile452 of **4** led to a 2.5-fold decrease in the antiviral activity [EC_{50} (**7**) = 0.023 μM]. Peptides **8**–**10** with further removal of single residues exhibited comparable submicromolar potency [EC_{50} (**8**) = 0.26 μM; EC_{50} (**9**) = 0.51 μM; EC_{50} (**10**) = 0.38 μM]. Peptide **11** exhibited much less potent antiviral activity [EC_{50} (**11**) = 1.2 μM]. As anticipated, at 10 μM, no activity was observed in peptides **12**–**14**, in which Leu457 was truncated. This lack of activity suggests that hydrogen bonds formed by the N-terminal non-helical region, including Leu457 in **4**, play critical roles in interactions with HR1. Because the main chain of Leu457 established two hydrogen bonds with Asn183 of HR1-42,[25] deletion of Leu457 in peptide **12** would cause marked changes in both antiviral activity and structural stability of the six-helical bundle with HR1 peptide.

In the CD spectroscopic analysis, five derivatives **7**–**11** with moderate to potent antiviral activity showed similar α-helical structure and thermal stability of the six-helical bundle with those of **4** (Fig. 4A–D, and Table 2). By contrast, three peptides **12**–**14**, which lacked antiviral activity, had substantially reduced $[\theta]_{222}$ values and showed a pronounced decrease in T_m values, indicating a compromised α-helix structure (Fig. 4E and F, and Table 2). These results suggest that Leu457 of peptide **11** may play a crucial role in the interaction with the HR1-derived peptide. Notably, the CD analysis results for these peptides did not correlate with their antiviral activity profile, likely because the N-terminal region of peptides **7**–**11** did not interact with HR1-40 under the conditions used for the CD analysis.

We next investigated the possible contributions of the upstream sequence of the HR2-derived peptide to the interaction with the HR1 region. For this purpose, three N-terminally extended peptides **15**–**17** were newly designed and synthesized, in which one to three residues were appended to the N-terminus of **4**. The antiviral activities of **15**–**17** were slightly higher than those of **4** [EC_{50} (**15**) = 0.0031 μM; EC_{50} (**16**) = 0.0042 μM; EC_{50} (**17**) = 0.0044 μM] (Table 3). The differences in CD spectra and T_m values between parent

Table 2 Antiviral activity and CD analysis of N-terminally truncated derivatives **7**–**14**

Peptide	Sequence	EC_{50}[a] (μM) [pEC$_{50}$ ± SD]		CD analysis	
				$[\theta]_{222}$[b]	T_m[c] (°C)
MEK28GT (**4**)	Ac-ISLERLDVGTNLKKAEEKLKKAEELLKK-NH_2	0.0092	[8.0 ± 0.3]	−16 507	45.7
7	Ac-SLERLDVGTNLKKAEEKLKKAEELLKK-NH_2	0.023	[7.6 ± 0.6]	−20 677	49.1
8	Ac-LERLDVGTNLKKAEEKLKKAEELLKK-NH_2	0.26	[6.6 ± 0.9]	−17 171	46.0
9	Ac-ERLDVGTNLKKAEEKLKKAEELLKK-NH_2	0.51	[6.3 ± 0.5]	−16 674	48.9
10	Ac-RLDVGTNLKKAEEKLKKAEELLKK-NH_2	0.38	[6.4 ± 0.8]	−16 135	48.6
11	Ac-LDVGTNLKKAEEKLKKAEELLKK-NH_2	1.2	[5.9 ± 0.3]	−20 103	49.4
12	Ac-DVGTNLKKAEEKLKKAEELLKK-NH_2	>10		−8222	26.6
13	Ac-VGTNLKKAEEKLKKAEELLKK-NH_2	>10		−6565	25.1
14	Ac-GTNLKKAEEKLKKAEELLKK-NH_2	>10		−7447	26.0

[a] The concentration required to inhibit viral replication by 50%. [b] Molar ellipticity at 222 nm of the six-helical bundles formed by the HR2-derived peptides in the presence of equimolar HR1-40. [c] T_m values are defined by the temperature at which half of the peptides are folded, and the other are unfolded.

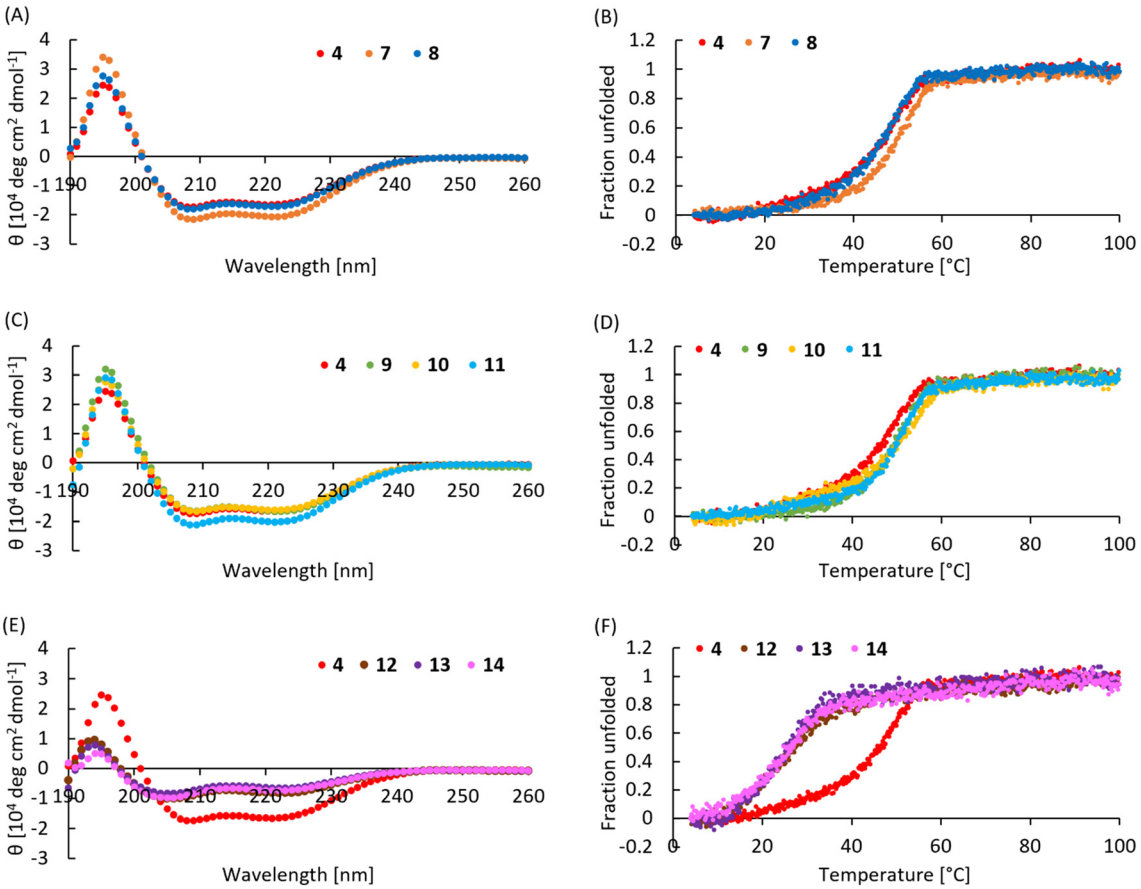

Fig. 4 CD analysis of peptides **4** and **7–14** in the presence of the HR1-40. (A), (C) and (E) CD spectra. (B), (D) and (F) Thermal stability of the six-helical bundles.

peptide **4** and extended peptides **15–17** were only marginal (Fig. S1 and Table 3), indicating that the thermal stability of the helical bundle structure with HR1-40 remained essentially unchanged. Notably, in the crystal structure of **1**/HR1-42 complex, the N-terminal non-helical region of **1** (Ile452-Glu455) extends beyond the C-terminus (Asn184) of the interacting HR1 trimer (Fig. 3). The similar thermal stability among peptides **4** and **15–17** may be due to the absence of involvement of the extended N-terminal residue(s) in **15–17** in the interaction with the HR1-40 trimer under the experimental conditions of the CD measurements.

Optimization of the interactive interface on HR2-derived peptides for the binding with HR1. Previously, we reported that substitution of Ser138 in enfuvirtide with alanine improved the antiviral activities against wild-type and enfuvirtide-resistant strains of HIV-1.[28] The crystallographic study and theoretical calculation of the six-helical bundle suggested that substitution with alanine decreased the desolvation free energy of the peptide to enhance the

Table 3 Antiviral activity and CD analysis of N-terminally extended derivatives **15–17**

Peptide	Sequence	EC_{50}[a] (μM) [pEC_{50} ± SD]		CD analysis	
				$[\theta]_{222}$[b]	T_m[c] (°C)
MEK28GT (**4**)	Ac-ISLERLDVGTNLKKAEEKLKKAEELLKK-NH_2	0.0092	[8.0 ± 0.3]	−14 508	39.4
15	Ac-PISLERLDVGTNLKKAEEKLKKAEELLKK-NH_2	0.0031	[8.5 ± 0.2]	−15 501	44.5
16	Ac-PPISLERLDVGTNLKKAEEKLKKAEELLKK-NH_2	0.0042	[8.4 ± 0.4]	−13 229	44.0
17	Ac-GPPISLERLDVGTNLKKAEEKLKKAEELLKK-NH_2	0.0044	[8.4 ± 0.4]	−12 606	42.3

[a] The concentration required to inhibit viral replication by 50%. [b] Molar ellipticity at 222 nm of the six-helical bundles formed by the HR2-derived peptides in the presence of equimolar HR1-40. [c] T_m values are defined by the temperature at which half of the peptides are folded, and the other are unfolded.

hydrophobic interaction with HR1 peptide.[29] We speculated that replacing the interactive residue(s) of MEK28GT (**4**) with more hydrophobic amino acid(s) would strengthen the interaction to improve the antiviral activity, at least potentially. To optimize the hydrophobic interface between peptide **4** and the HR1 trimer, five derivatives were designed and synthesized by replacing the nonpolar amino acids (Ala466, Ala473, Leu463, Leu470, and Leu477) at the interface with the HR1 trimer with those bearing more hydrophobic side chains. Their antiviral activities were evaluated, and the stability of the helical bundle with HR1-40 was assessed by CD spectroscopy. (Table 4 and Fig. 5). The antiviral activity of peptide **18**, in which Ala was substituted with Val, was comparable to that of **4**, whereas peptide **19** exhibited 2.5-fold lower antiviral activity compared with **4** [EC_{50} (**18**) = 0.010 μM; EC_{50} (**19**) = 0.023 μM]. Furthermore, peptides **20**–**22**, in which Leu residues at the interaction interface were replaced with Phe, also exhibited significantly less potent antiviral activity of **4**. These results suggest that four residues (Ala473, Leu463, Leu470, and Leu477) are indispensable for the antiviral activity. Their hydrophobic side chains at the HR1-facing interface of peptide **4** appear well suited to interact with the hydrophobic pockets on the HR1 coiled-coil. Replacement of Ala466 in **4** with bulkier hydrophobic side chains was tolerated without improving antiviral activity (peptide **18**), but resulted in reduced activity in other derivatives (peptides **19**–**22**), presumably owing to steric constraints at the binding interface. The T_m values of peptides **18**–**22** were lower than those of **4**; however, no clear correlation

Table 4 Antiviral activity and CD analysis of derivatives **18**–**23** with substitutions at the interaction interface

Peptide	Sequence	EC_{50}[a] (μM) [pEC_{50} ± SD]		CD analysis	
				$[\theta]_{222}$[b]	T_m[c] (°C)
MEK28GT (**4**)	Ac-ISLERLDVGTNLKKAEEKLKKAEELLKK-NH_2	0.0092	[8.0 ± 0.3]	−9844	45.5
18	Ac-ISLERLDVGTNLKK**V**EEKLKKAEELLKK-NH_2	0.010	[7.9 ± 0.5]	−6841	28.3
19	Ac-ISLERLDVGTNLKKAEEKLKK**V**EELLKK-NH_2	0.023	[7.6 ± 0.3]	−8866	37.2
20	Ac-ISLERLDVGTN**F**KKAEEKLKKAEELLKK-NH_2	4.8	[5.3 ± 0.1]	−3562	23.2
21	Ac-ISLERLDVGTNLKKAEEK**F**KKAEELLKK-NH_2	0.12	[6.9 ± 0.7]	−8698	36.3
22	Ac-ISLERLDVGTNLKKAEEKLKKAEEL**F**KK-NH_2	0.049	[7.3 ± 0.5]	−6259	27.4
23	Ac-ISLERLDVGTNLKKAEEKLKKAEELLKK**S**-NH_2	0.0046	[8.3 ± 0.5]	−12 499	52.7

[a] The concentration required to inhibit viral replication by 50%. [b] Molar ellipticity at 222 nm of the six-helical bundles formed by the HR2-derived peptides in the presence of equimolar HR1-40. [c] T_m values are defined by the temperature at which half of the peptides are folded, and the other are unfolded.

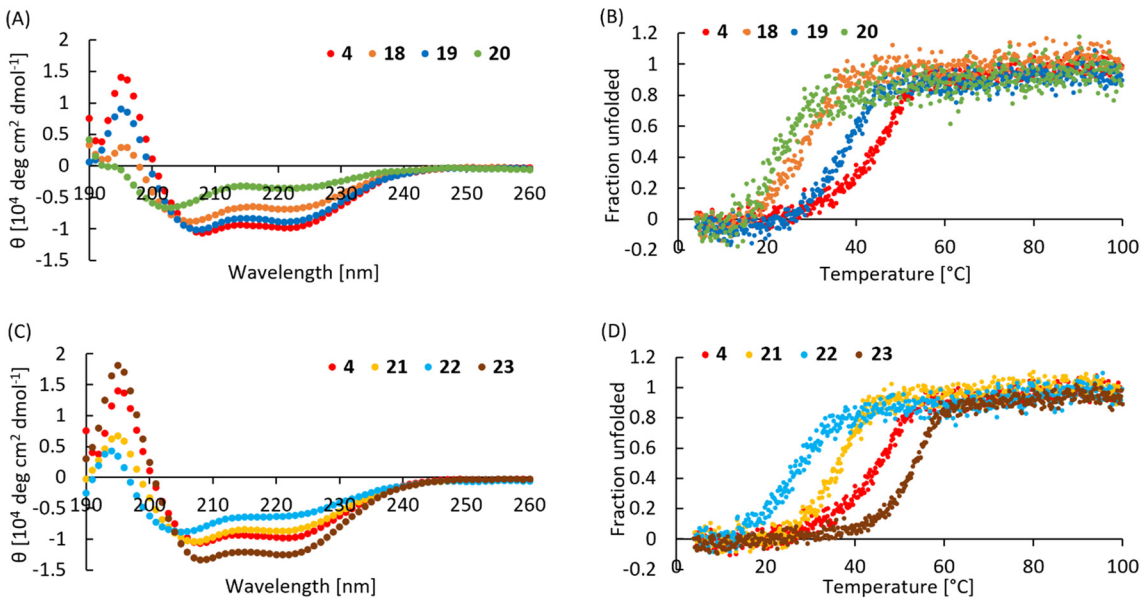

Fig. 5 CD analysis of peptides **4** and **18**–**23** in the presence of HR1-40. (A) and (C) CD spectra. (B) and (D) thermal stability of the six-helical bundles.

with antiviral activity was observed. Notably, peptide **22** exhibited the highest activity among the three Leu-substituted peptides **20**–**22**, whereas this had a lower T_m than the less potent **21**. The somewhat different CD spectra of peptides **20** and **22** may feature their distinct secondary structures.

Peptide **23** was also designed, in which Ser480 was appended at the C-terminus of MEK28GT (**4**). In the crystal structure of MEK35GT (**3**)/HR1-42 complex, Ser480 formed two hydrogen bonds with Ser153 and Thr157 of HR1 peptide.[25] Peptide **23** exhibited comparable antiviral activity to that of **4**, whereas the thermal stability (T_m) was increased. This finding indicates that Ser480-mediated hydrogen bonds would contribute to the stability of the helical bundle with the HR1 peptide but would not directly affect antiviral activity.

Investigation of the thermal stability of the potential six-helical bundles. During our structure–activity relationship studies, we found that the thermal stability (T_m values) of MEK28GT derivatives in the presence of HR1-40 was poorly correlated with antiviral activity. Especially in the case of the N-terminally truncated derivatives, the T_m values of peptides **7**–**11** were essentially similar, although the antiviral activity varied with the truncations (Table 2). We assumed that this poor structure–property correlation might be attributed to the missing counterpart region in the HR1-derived peptide HR1-40 during interaction with MEK28GT derivatives. To address this issue, two extended HR1 peptides, HR1X and HR1Y, were designed and synthesized (Table 5). HR1X and HR1Y contain an additional sequence of seven and ten residues at the C-terminus of HR1-40, respectively. In the cryo-EM structure of the postfusion state, this additional sequence of an α-helix structure forms the groove to accept the sidechains of Ile452 and Leu454.[21]

CD spectrum and T_m value of peptide **4** were measured in the presence of each HR1-derived peptide (Table 6 and Fig. 6). To enable direct comparison with the newly synthesized HR1 derivatives, HR1-40 was also reinvestigated under identical conditions, consistent with the data presented above (Tables 1 and 3). When HR1X was used for the CD analysis, a higher α-helix property was observed in the spectrum compared with that of HR1-40 [$[\theta]_{222}$ (**4**/HR1X) = −23 210] (Fig. 6A). The thermal stability of the peptide **4**/HR1X complex was higher than that of the HR1-40 complex in the analysis of the temperature-dependent changes in $[\theta]_{222}$ [T_m (**4**/HR1X) = 68.8 °C] (Fig. 6C). The T_m value of peptide **4** in the presence of HR1Y was even higher than that obtained in the presence of HR1X [T_m (**4**/HR1Y) = 71.8 °C] (Fig. 6C), whereas the α-helicity was similar to that of the **4**/HR1-40 complex [$[\theta]_{222}$ (**4**/HR1Y) = −16 865]. These results indicate that the extended C-terminal region in HR1X and HR1Y would interact with the N-terminal region of **4**, thereby enhancing the stability of the six-helical bundle. Notably, **3**/HR1X and **3**/HR1Y complexes did not undergo complete denaturation in the measured temperature range (4–100 °C) (Fig. 6B). The T_m values calculated from the fraction of unfolded peptide, based on the mean residue molar ellipticity at the beginning and end of the measurement, do not accurately reflect the actual thermal stability of the **3**/HR1X complex (Fig. 6C).

Table 5 Sequences of HR1 derivatives

Peptide	Sequence
HR1-40	Ac-QAIDNLRASLETTNQAIEAIRQAGQEMILAVQGVQDYINN-NH_2
HR1X	Ac-QAIDNLRASLETTNQAIEAIRQAGQEMILAVQGVQDYINNELIPSMN-NH_2
HR1Y	Ac-QAIDNLRASLETTNQAIEAIRQAGQEMILAVQGVQDYINNELIPSMNQLS-NH_2

Table 6 Antiviral activity and CD analysis of HR2 derivatives in the presence of HR1 derivatives

Peptide	EC_{50} (μM)[a] [pEC_{50} ± SD]		CD analysis HR1–40 $[\theta]_{222}$[b]	CD analysis HR1–40 T_m (°C)[c]	CD analysis HR1X $[\theta]_{222}$[d]	CD analysis HR1X T_m (°C)[c]	CD analysis HR1Y $[\theta]_{222}$[e]	CD analysis HR1Y T_m (°C)[c]
MEK35GT (**3**)	0.0021	[8.7 ± 0.3]	−17 863	84.4	−24 259	–[f]	−18 466	–[f]
MEK28GT (**4**)	0.0092	[8.0 ± 0.3]	−14 771	46.0	−23 210	68.8	−16 865	71.8
15	0.0031	[8.5 ± 0.2]	−17 803	49.3	−23 875	69.8	−18 179	73.5
16	0.0042	[8.4 ± 0.4]	−12 080	42.3	−21 442	–[g]	−14 847	67.8
17	0.0044	[8.4 ± 0.4]	−12 903	44.6	−20 806	–[g]	−14 863	70.4

[a] The concentration required to inhibit viral replication by 50%. [b] Molar ellipticity at 222 nm of the six-helical bundles formed by the HR2-derived peptides in the presence of equimolar HR1-40. [c] T_m values are defined by the temperature at which half of the peptides are folded, and the other are unfolded. [d] Molar ellipticity at 222 nm of the six-helical bundles formed by the HR2-derived peptides in the presence of equimolar HR1X. [e] Molar ellipticity at 222 nm of the six-helical bundles formed by the HR2-derived peptides in the presence of equimolar HR1Y. [f] T_m values could not be determined because unfolding was incomplete within the examined temperature range; even at the maximum temperature (100 °C), the absolute values of $[\theta]_{222}$ remained relatively large (Fig. 6B). [g] T_m values could not be determined because the unfolding process did not follow a single cooperative transition, but rather exhibited biphasic behavior in the temperature-dependent CD measurements (Fig. 7C).

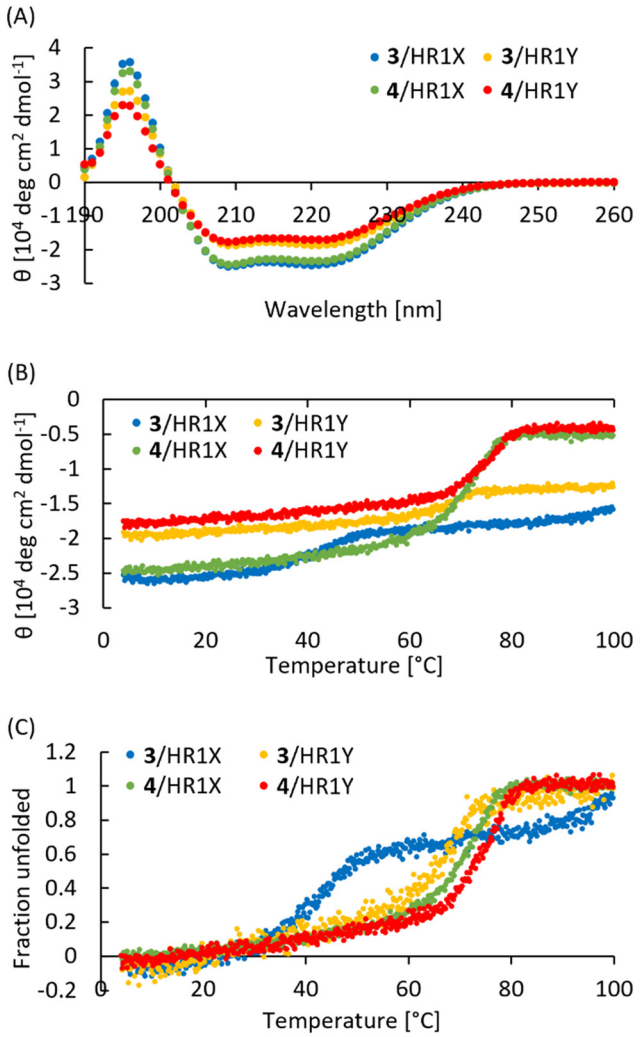

Fig. 6 CD analysis of peptides **3** and **4** in the presence of the HR1X or HR1Y. (A) CD spectra. (B) Molar ellipticity at 222 nm of the six-helical bundle. (C) Thermal stability of the six-helical bundle.

It is unlikely that HR1X and HR1Y can accurately determine the T_m value of MEK35GT derivatives.

Using the newly designed HR1 peptides, the helical properties of N-terminally extended peptides **15–17** were investigated (Fig. 7 and Table 6). The CD spectra of peptides **15–17** in the presence of HR1X or HR1Y were similar to that of peptide **4** (Fig. 7A and B). In the thermal denaturation profiles of **16**/HR1X and **17**/HR1X complexes, biphasic transitions were observed upon heating, which prevented the accurate estimation of T_m values (Fig. 7C and E, and Table 6). Notably, unlike the HR1X complexes, the thermal denaturation profiles of these three complexes of **15–17** with HR1Y did not display biphasic transitions (Fig. 7D and F). The complexes of peptides **15–17** with HR1Y exhibited high T_m values, similar to those of **4**/HR1Y complex [T_m (**15**/HR1Y) = 73.5 °C; and T_m (**16**/HR1Y) = 67.8 °C; T_m (**17**/HR1Y) = 70.4 °C]. These results indicate that HR1Y would be a more appropriate HR1 peptide to assess the thermal stability of complexes with N-terminally extended derivatives of **4**.

Using HR1Y, we reinvestigated the secondary structure and thermal stability of the complexes formed with the N-terminally truncated derivatives **7–14** (Table 7 and Fig. 8). The CD spectra in the presence of HR1Y were similar among peptides **4** and **7–14** (Fig. 8A and B). The CD thermal denaturation experiments revealed that peptide **7**, with a single N-terminal truncation at **4**, showed a marked decrease in T_m compared with peptide **4** [T_m (**7**/HR1Y) = 63.2 °C]. The temperature-dependent ellipticity profile exhibited a gradual transition around 50 °C, suggesting that the T_m value may be underestimated. The **8**/HR1Y complex retained comparable thermal stability of **4** [T_m (**8**/HR1Y) = 70.7 °C], although the antiviral activity of **8** was 28-fold less potent than **4**. The T_m values of **9–11** with less potent activity were significantly lower than **4** (T_m = 60.6–61.3 °C). Peptides **12–14** showed a further reduction in the stability of the six-helical bundles (T_m = 51.6–53.1 °C). These findings indicate that thermal stability measurements using HR1Y provide a more reliable reflection of the structure–activity relationships than those obtained with HR1-40, and that the extended C-terminal region of HR1Y likely interacts with the N-terminal region of **4**, as anticipated.

In previous studies on fusion inhibitors, several modifications and manipulations of HR1 peptides were attempted to investigate the secondary structure and thermal stability of potential six-helical bundles. For example, enfuvirtide, an HIV fusion inhibitor, cannot form a stable six-helical bundle with HR1-derived peptides, which hampers analysis of the interaction by CD spectroscopy.[30] To overcome this limitation, a 5-helix design strategy using a molecular mimic of the HIV-1 gp41 coiled-coil structure was employed for structure–activity relationship studies.[31] In the assessment of secondary structures of the HR1–HR2 complex of severe acute respiratory syndrome coronavirus 2 (SARS-CoV-2), a trimerization motif of T4 bacteriophage fibritin-foldon was conjugated at the C-terminus of the HR1 peptide to stabilize the HR1 trimer.[32] In the present study, the correlation between T_m values and antiviral activity is dependent on the HR1 model used in the assay system. These findings indicate that secondary structure and thermal stability measurements depend on the use of an appropriate HR1 model to capture the interaction of HR2-derived peptides fully. Thus, T_m values can serve as a valuable indicator for evaluating the interaction with the viral HR1 trimer when an appropriate HR1 model is employed.

Molecular modeling analysis of the six-helical bundle formed by MEK28GT and HR1Y. In our X-ray crystallographic analysis, the N-terminal region of MV HR2-derived peptides adopts a non-helical conformation.[25] Introduction of α-helix-inducing X-EE-XX-KK motifs into this non-helical region reduced the antiviral activity, suggesting that maintaining a non-helical structure in this N-terminal region is important for bioactivity. However, the contributions of individual residues in this region to the interaction(s) remain unclear, because short HR1 peptides such as HR1-40 and HR1-42 were used.[25]

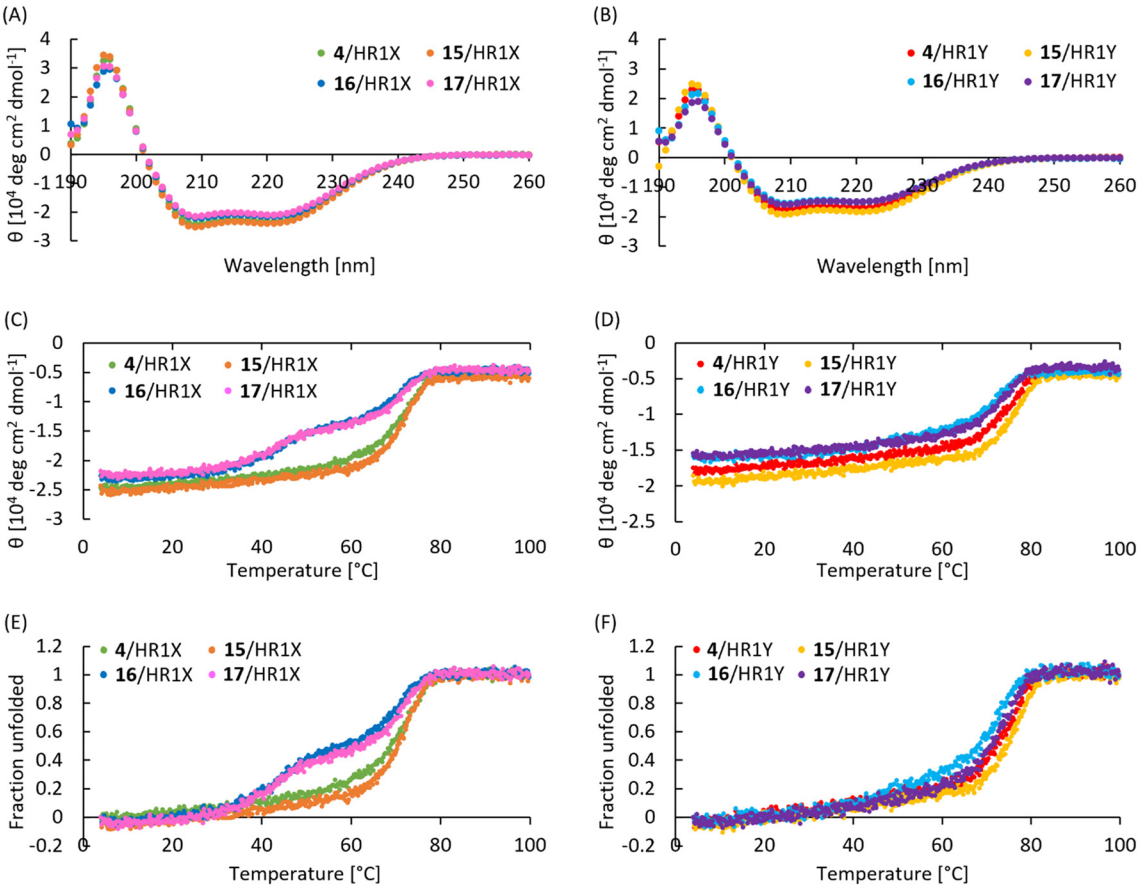

Fig. 7 CD analysis of peptides **4** and **15–17** in the presence of the HR1X or HR1Y. (A) and (B) CD spectra. (C) and (D) Molar ellipticity at 222 nm of the six-helical bundle. (E) and (F) Thermal stability of the six-helical bundle.

Table 7 Antiviral activity and CD analysis of N-terminally extended derivatives **7–14** in the presence of HR1Y

Peptide	EC_{50} (μM)[a] [pEC_{50} ± SD]		CD analysis HR1–40 $[\theta]_{222}$[b]	CD analysis HR1–40 T_m (°C)[c]	CD analysis HR1Y $[\theta]_{222}$[d]	CD analysis HR1Y T_m (°C)[c]
MEK28GT (**4**)	0.0092	[8.0 ± 0.3]	−16 507	45.7	−23 372	72.3
MEK28GT-1 (**7**)	0.023	[7.6 ± 0.6]	−20 677	49.1	−21 671	63.2
MEK28GT-2 (**8**)	0.26	[6.6 ± 0.9]	−17 171	46.0	−23 863	70.7
MEK28GT-3 (**9**)	0.51	[6.3 ± 0.5]	−16 674	48.9	−23 744	60.6
MEK28GT-4 (**10**)	0.38	[6.4 ± 0.8]	−16 135	48.6	−23 284	61.3
MEK28GT-5 (**11**)	1.2	[5.9 ± 0.3]	−20 103	49.4	−24 400	61.0
MEK28GT-6 (**12**)	>10		−8222	26.6	−22 378	53.1
MEK28GT-7 (**13**)	>10		−6565	25.1	−20 469	52.5
MEK28GT-8 (**14**)	>10		−7447	26.0	−21 187	51.6

[a] The concentration required to inhibit viral replication by 50%. [b] Molar ellipticity at 222 nm of the six-helical bundles formed by the HR2-derived peptides in the presence of equimolar HR1-40. [c] T_m values are defined by the temperature at which half of the peptides are folded, and the other are unfolded. [d] Molar ellipticity at 222 nm of the six-helical bundles formed by the HR2-derived peptides in the presence of equimolar HR1Y.

To investigate interactions between the N-terminal region of HR2-derived peptides and the extended C-terminal region of HR1Y, we constructed a molecular model of the MEK28GT (**4**)/HR1Y complex using homology modeling in the molecular operating environment (MOE). In our previous report on the crystal structure of MEK35GT (**3**) in complex with HR1-42 (PDB ID: 8XO8),[25] there was no C-terminal region in the HR1 peptides (HR1-40 and HR1-42) for interacting with the N-terminal non-helical sequence (Ile452-Leu454) of **3**. To accommodate the missing data on their interaction modes, the structural templates for the C-terminal extension in HR1Y and the N-terminal non-helical region in **4** were needed. We used the crystal structure of the **3**/HR1-42 complex and the postfusion six-helical bundle structure of

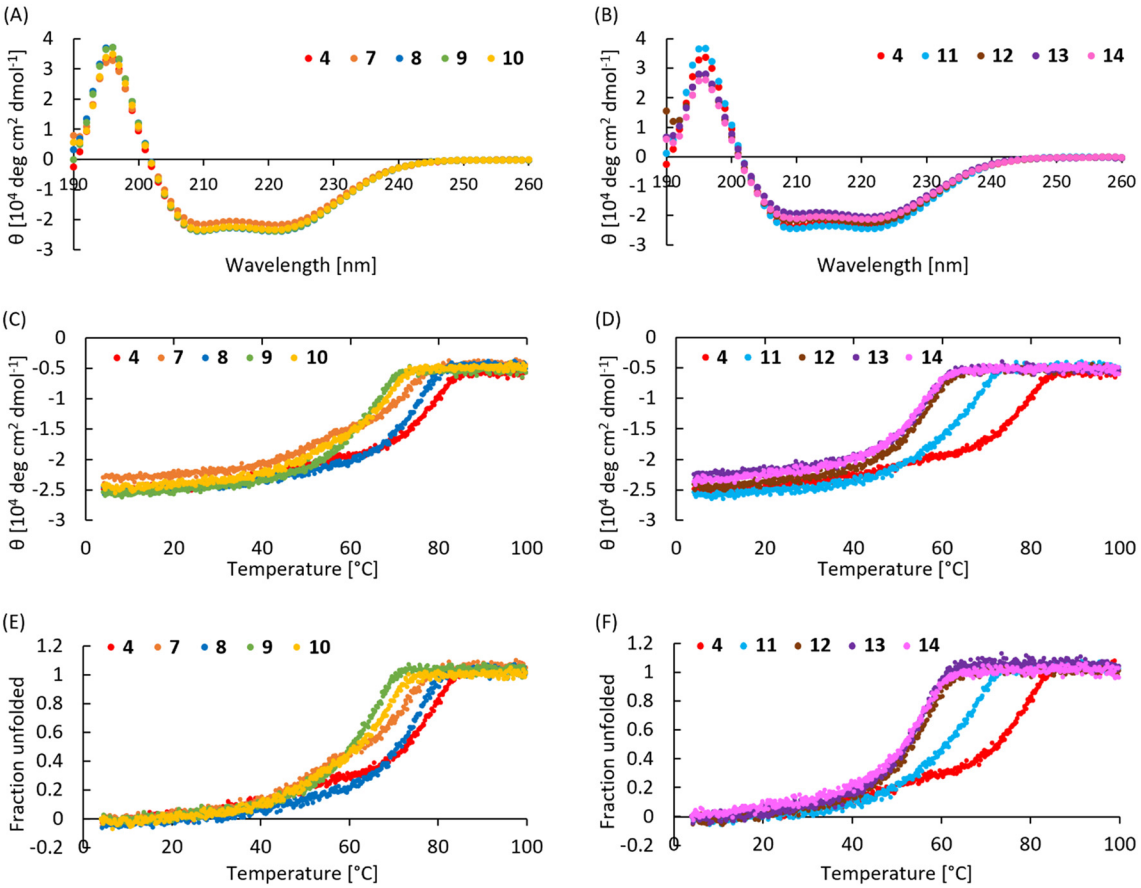

Fig. 8 CD analysis of peptides **4** and **7**–**14** in the presence of the HR1Y. (A) and (B) CD spectra. (C) and (D) Molar ellipticity at 222 nm of the six-helical bundle. (E) and (F) Thermal stability of the six-helical bundle.

the MV F protein determined by cryo-EM (PDB ID: 8UTF)[21] as complementary templates. The common region of HR1-40 and HR1Y (Gln145-Asn184) was modeled based on the crystal structure of the **3**/HR1-42 complex, whereas the C-terminally extended region in HR1Y (Glu185-Ser194) was modeled using the postfusion cryo-EM structure. Similarly, the α-helical structure of X-EE-XX-KK motifs in **4** and the N-terminal non-helical region were based on their crystal and cryo-EM structures, respectively. To model the N-terminal non-helical region of **4** appropriately in the presence of the extended HR1, we sequentially generated homology models of HR1Y followed by **4**, yielding a final model of the **4**/HR1Y complex (Fig. 9).

In this final model, the α-helical region of **4** (Gly460-Lys479) was accommodated in the groove formed by the HR1 trimer, in which the interaction mode was consistent with that of the **3**/HR1-42 complex. The groove shape of HR1 trimer was collapsed at a small disordered kink around Tyr181 to form a steric wall by the side chain on the cavity (Fig. 9A and B). The N-terminal non-helical region of **4** overrode the bump in an extended conformation (Fig. 9C). In the non-helical region, the backbone amides of Leu454, Glu455, Leu457, and Val459 participated in intermolecular hydrogen bondings with the side chains of Asn191, Tyr181, Asn183, and Gln179, respectively (Fig. 9C). Additionally, the Arg456 side chain involved the interaction with the side chains of Asp180 and Asn184, whereas the Asp458 side chain formed a hydrogen bond with the Gln179 side chain. The side chains of Ile452, Leu454, Leu457, and Val459 occupied hydrophobic cavities on the surface of the HR1 trimer, making hydrophobic contacts. Notably, Ile452 and Leu454, which had no appreciable interactions with the HR1 region in the **3**/HR1-42 structure, were buried in the hydrophobic cavities located beyond Tyr181 (Fig. 9D).

These interaction features in the homology model of **4**/HR1Y were compared with those in the postfusion MV F protein structure (PDB ID: 8UTF) (Fig. 9E and F). Overall, the interaction pattern was highly conserved. For example, the side chains of four hydrophobic residues (Ile452, Leu454, Leu457, and Val459) occupied similar positions to those of the corresponding residues in the postfusion structure. No substantial differences were observed in the positions of Ser453 and Arg456 side chains. In contrast, several local differences in side-chain orientations and contact residues were evident. The orientation of the Asp458 side chain differed markedly (Fig. 9F). The interactions of Arg456 and Asp458 with Gln179, Asp180, and Asn184 in **4**/HR1Y were not observed in the postfusion structure. This absence may be

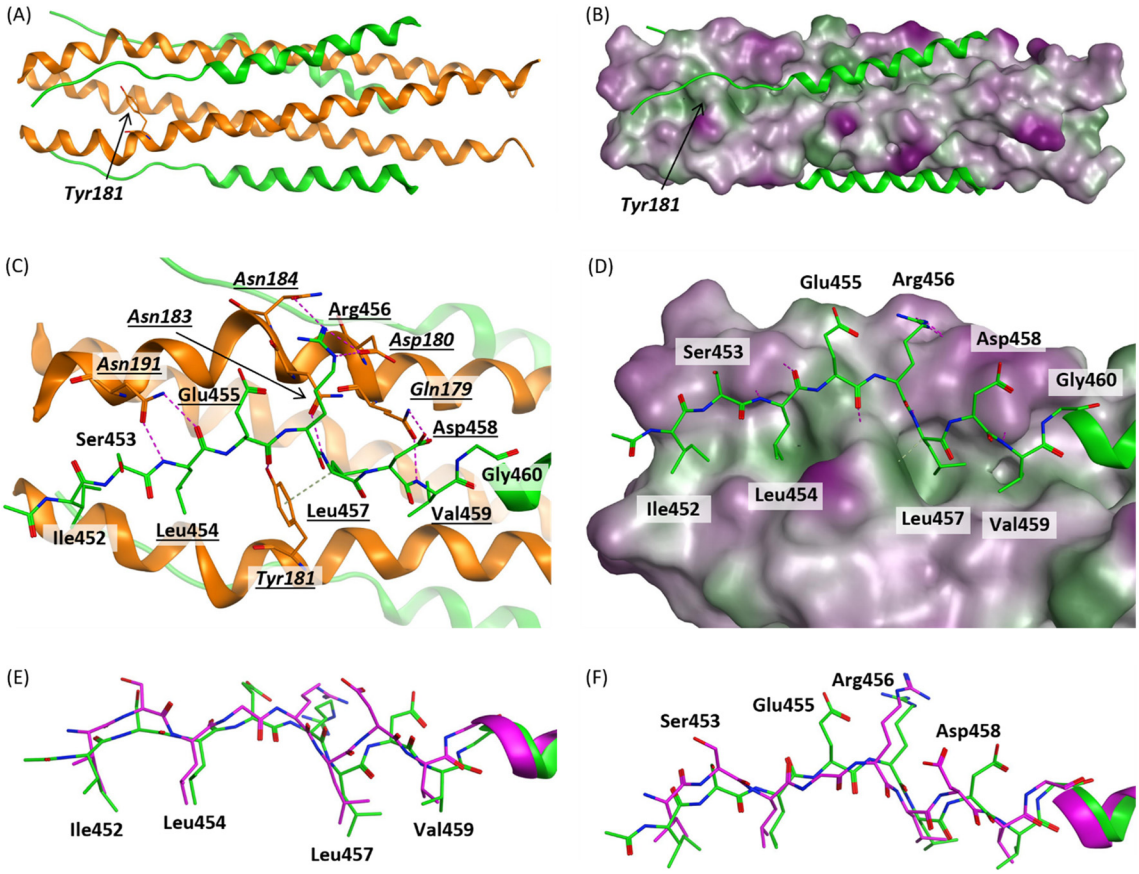

Fig. 9 Molecular models of the six-helical bundle formed by peptide **4** (green) and HR1Y (orange). HR1Y residues are shown in italics. (A) Overall view of the six-helical bundle. (B) Overall view of the six-helical bundle with the surface of the HR1Y trimer rendered according to lipophilicity (purple, hydrophilic; gray, neutral; green, lipophilic). (C) Close-up view of the N-terminal region of **4**. Residues involved in hydrogen bonding are underlined. (D) Close-up view of the N-terminal region of **4** with the surface of the HR1Y trimer rendered according to lipophilicity. (E and F) superposition of the N-terminal region of **4** with the corresponding region in the postfusion MV F protein structure (PDB ID: 8UTF, purple).

due to the lack of the side chain at position 455 (Gly) in the MV F protein structure, which was an experimental manipulation to stabilize the postfusion structure. These observations indicate that the homology model of **4**/HR1Y reasonably retained the key interactions observed in the postfusion MV F protein structure.

Next, we analyzed the structure–activity relationships of a series of MEK28GT derivatives in the context of the homology model. Deletion of Ile452 in peptide **4** led to a 2.5-fold reduction in activity relative to **4** [EC_{50} (**7**) = 0.023 μM], consistent with the loss of the key hydrophobic interaction involving Ile452 identified in the model. Removal of Ser453 in peptide **7** also resulted in a pronounced 10-fold decrease in activity compared with **7** [EC_{50} (**8**) = 0.26 μM]. This decrease suggests that Ser453 may also make a significant contribution to antiviral activity, although the direct interaction between Ser453 and HR1Y was not observed in the model. It was of interest to note that deletion of Leu454 in peptide **8** caused little effect on the antiviral activity [EC_{50} (**9**) = 0.51 μM], although Leu454 formed apparently critical interactions with HR1Y *via* binding with a hydrophobic pocket in the groove, as well as two hydrogen bonds with the Asn191 side chain. These observations suggest that Ser453 and Leu454 cooperatively contribute to the antiviral activity, in which the presence of Ser453 underpins the beneficial interactions of Leu454 with the hydrophobic pocket behind the Tyr181 bump. Deletion of Glu455 in peptide **9** had only a minimal effect on the antiviral activity and the thermal stability [EC_{50} (**10**) = 0.38 μM; T_m (**10**/HR1Y) = 61.3 °C], although the main chain carbonyl group of Glu455 in **9** formed a hydrogen bond with Tyr181 phenol OH. This minimal effect suggests that the contribution of apparent hydrogen bonding may be significantly less. Removal of Arg456 in peptide **10** resulted in an approximately 3-fold reduction in antiviral activity [EC_{50} (**11**) = 1.2 μM], which is consistent with the intermolecular hydrogen bonding of Arg456 with Asn184 and Asp180 in HR1Y. The side chain of Leu457 occupies a deep hydrophobic pocket on the HR1Y trimer, and its backbone NH forms a hydrogen bond with the Asn183 side chain. The loss of these interactions likely accounts for the pronounced reduction in the antiviral activity of peptide **12** [EC_{50} (**12**) >10 μM].

In the thermal stability measurements using HR1Y, there was no appreciable change in T_m values between peptide **4**

and N-terminally extended peptides **15–17** [T_m (**15**/HR1Y) = 73.5 °C; T_m (**16**/HR1Y) = 67.8 °C; T_m (**17**/HR1Y) = 70.4 °C]. This lack of change may be due to an absence of binding site(s) in HR1Y for the Gly449-Pro451 region in **15–17** in productive interactions, whereas the N-terminal Ile452 in **4** is buried in the groove at the C-terminal edge of the HR1Y trimer formed by Ser189, Met190, and Gln192-Ser194. Therefore, extending the N-terminal region in peptide **4** did not further stabilize the complex with HR1Y, and no correlation was observed between antiviral activity and thermal stability. To validate this interpretation, a homology model of the complex between **17** and an HR1 derivative with further extension of eight residues at the C-terminus of HR1Y was generated using the same procedure (Fig. S2). In this model, the Pro451 side chain contacted the HR1 trimer surface, suggesting that Pro451 may participate in hydrophobic interactions. By contrast, although Pro450 and Gly449 are arranged along the HR1 trimer surface, no clear interactions involving these residues were observed. These observations are consistent with the antiviral activity profile, in which the addition of Pro451 to peptide **4** resulted in an approximately 3-fold increase in activity relative to **4** [EC_{50} (**15**) = 0.0031 μM], whereas further extension with Pro450 and Gly449 had little effect on antiviral activity [EC_{50} (**16**) = 0.0042 μM; EC_{50} (**17**) = 0.0044 μM]. Taken together, this molecular model successfully accounts for the structure–activity relationships of a series of MEK28GT derivatives, particularly those involving Pro451, Ile452, Arg456, and Leu457. These findings suggest that rational modification of HR2-derived peptides should preserve key interactions in the N-terminal non-helical region rather than simply enhancing α-helical stability.

Conclusions

In this study, the structure–activity relationships of HR2-region-derived peptides derived from the MV F protein were investigated. We identified MEK28GT (**4**) as a minimal membrane-fusion-inhibitory peptide that retains potent anti-MV activity through interaction with the HR1 region of the viral F protein. SAR analyses revealed several key residues in the HR2-derived peptide, highlighting both hydrophobic and polar contributions to HR1–HR2 binding. Using HR1Y, a C-terminally extended HR1 derivative, the thermal stabilities of the potential six-helical bundles were measured more accurately to reflect the structure–activity relationships by the N-terminal truncations from peptide **4**. We demonstrated that interactions between the N-terminal region of HR2-derived peptides and the C-terminal region of HR1 peptides substantially influenced the six-helical bundle stability. Molecular modeling of the **4**/HR1Y complex rationalized the structure–activity and structure–property relationships, particularly the loss of antiviral activity by deletion of Ile452, Arg456, and Leu457. Taken together, these findings suggest that appropriate evaluation of peptide–HR1 region interactions benefits from the use of newly designed HR1Y. Through these investigations, the structural basis underlying the contribution of the N-terminal region to antiviral activity was clarified, which was not resolved in the X-ray crystal structures reported in our previous work. The structure–activity relationship data in this study would provide new insights to guide further optimization of fusion-inhibitory peptides against MV.

Experimental

Peptide synthesis and purification

Reagents and solvents were purchased from Watanabe Chemical Industries, Ltd. (Hiroshima, Japan), Kokusan Chemical Industries, Ltd. (Kanagawa, Japan), Sigma-Aldrich JAPAN (Tokyo, Japan), Wako Pure Chemical Industries, Ltd. (Osaka, Japan), Tokyo Chemical Industry Co., Ltd. (Tokyo, Japan) or Nacalai Tesque, Inc. (Kyoto, Japan). All peptides were synthesized by standard Fmoc-based solid-phase peptide synthesis (Fmoc-SPPS) on Rink Amide resin or NovaSyn TGR resin using an automatic microwave peptide synthesizer [Liberty BLUE (CEM Japan, Tokyo, Japan)] or an automatic peptide synthesizer [PSSM-8 (Shimadzu, Kyoto, Japan)]. Fmoc-protected amino acids had the following sidechain protections: *t*-butyl ester for Asp and Glu; trityl for Asn and Gln; *t*-butyloxycarbonyl (Boc) for Lys; 2,2,4,6,7-pentamethyldihydrobenzofuran-5-sulfonyl (Pbf) for Arg; *t*-butyl ether for Ser, Thr, and Tyr. Fmoc-protected amino acids (5 equiv.) were coupled using OxymaPure (10 equiv.)/DIC (5 equiv.) in DMF, and Fmoc deprotection was performed with 20% piperidine in DMF. The N-terminal of peptides was acetylated using acetic anhydride (10 equiv.) and pyridine (10 equiv.) in DMF. After chain assembly, the resulting protected peptide resin was treated with TFA/H_2O/*m*-cresol/thioanisole/1,2-ethanedithiol (80 : 5 : 5 : 5 : 5) at room temperature for 2 h. After removal of the resin by filtration, the filtrate was poured into ice-cold dry Et_2O. The resulting powder was collected by centrifugation and then washed twice with ice-cold dry Et_2O. The crude product was purified by high-performance liquid chromatography (HPLC) on a Cosmosil 5C_{18}-ARII preparative column (Nacalai Tesque Inc., Kyoto, Japan, 20 mm × 250 mm) with a linear gradient of CH_3CN containing 0.05% (v/v) TFA aq. at a flow rate of 8 mL min^{-1}, affording the expected peptides as freeze-dry white powder. For analytical HPLC of peptides, a Cosmosil 5C_{18}-ARII column (Nacalai Tesque, 4.6 × 250 mm) was employed with a linear gradient of CH_3CN containing 0.05% (v/v) TFA aq. at a flow rate of 1 mL min^{-1} (Fig. S3). All peptides were characterized by ESI-MS [LCMS-2020 (Shimadzu, Kyoto, Japan)] (Table S2).

Anti-MV activity

Antiviral assays were conducted as previously described.[26] B95a cells were used in all the experiments. The medium consisted of Roswell Park Memorial Institute 1640 medium supplemented with 1% fetal bovine serum, penicillin G (100

IU mL^{-1}), streptomycin (50 μg mL^{-1}), and varying concentrations of the compound (0.0001 to 10 μM). Cells were seeded into 96-well plates at 1×10^5 cells per well and inoculated with the human MV Edmonston strain. The cells were incubated at 37 °C in an incubator under an atmosphere of 5% CO_2 for 8 days. In these assays, wells cultured with virus and without compounds served as positive controls, and wells cultured without virus and without compounds served as negative controls. After incubation, the cell viability was determined using an MTT assay. The EC_{50} of favipiravir was 40 μM ($pEC_{50} = 4.4 \pm 0.2$) in this assay.[33]

CD measurement

CD measurements were performed by using a CD spectrometer (J-1500, JASCO) with a thermoelectric temperature controller. A stock solution of each peptide was prepared by dissolving the peptide in 2,2,2-trifluoroethanol (TFE) at a concentration of 0.5 mM. For a CD measurement of a 1 : 1 mixture of an HR1 peptide and an HR2-derived peptide, the mixture of the peptide stock solutions was made up to the final concentration of both the HR1 and HR2 peptides (10 μM) with PBS (pH 7.4) and incubated at 37 °C for 30 min. The wavelength dependence of molar ellipticity [θ] was monitored at 25 °C as the average of four scans, and the thermal stability of the HR1 and HR2 mixture was estimated by monitoring the change in the CD signal at 222 nm. The midpoint of the thermal unfolding transition (melting temperature [T_m]) of each complex was determined from the temperature dependence of $[\theta]_{222}$. The $[\theta]_{222}$ values measured over the temperature range of 4–100 °C at 0.2 °C intervals were smoothed using a five-point moving average. The baseline values were defined as the average of five consecutive data points at the lowest and highest temperature regions, respectively, and the data were then normalized to a scale from 0 (low-temperature baseline) to 1 (high-temperature baseline). A continuous region of the normalized data with values between 0.3 and 0.7 was selected, provided that the data exhibited a monotonic transition within this range. Linear regression analysis was performed on this region, and the temperature corresponding to a normalized value of 0.5 on the fitted line was defined as the T_m.

Homology modeling of six-helical bundle structures

A homology model of the MEK28GT (**4**)/HR1Y complex was constructed using the "Homology Model" tool in MOE (Chemical Computing Group, Montreal, Canada). All calculations were performed using the Amber:EHT force field implemented in MOE. For HR1Y modeling, the sequence of HR1Y was aligned with HR1-42 (PDB ID: 8XO8) and the HR1 region from the postfusion conformation of the MV F protein (PDB ID: 8UTF). HR1-42 from 8XO8 was used as the template, with residues 183–194 of the HR1 region from 8UTF as a template override to model the C-terminal extension absent in 8XO8. Residues 457–486 of MEK35GT (**3**) from 8XO8 and surrounding water molecules were defined as environmental atoms (kept fixed during modeling), and the refinement parameter was set to 0.5 (default setting). The generalized born/volume integral (GB/VI) score was used for model scoring, and the structure with the lowest score was selected. To alleviate potential local distortions in the constructed model, hydrogen atoms were energy-minimized and subsequently inspected for steric clashes. Because no significant steric clashes were detected, no additional energy minimization was performed. The N-terminus and C-terminus of HR1Y were manually acetylated and amidated, respectively. The resulting model contained the HR1Y homology model, residues 457–486 of **3** from 8XO8, and associated water molecules.

Subsequently, the sequence of **4** was aligned with residues 457–486 of **3**, contained in the HR1Y model, and with the HR2 region from 8UTF. A homology model of **4** was generated using residues 457–486 of **3** from the HR1Y model as the primary template, with residues 452–458 of the HR2 region from 8UTF used as a template override. The homology-modeled HR1Y and the surrounding water molecules were treated as environmental atoms, and all other modeling parameters were kept as described above. Hydrogen-only energy minimization and steric-clash inspection were also performed, and no additional energy minimization was applied because no significant steric clashes were detected. Finally, the N- and C-termini of **4** were manually acetylated and amidated, respectively. The final structure was taken as the homology model of the **4**/HR1Y complex.

A homology model of the complex between MEK28GT+3 (**17**) and an HR1 derivative with further extension of eight residues at the C-terminus of HR1Y (HR1Y+8) was constructed using the same procedure described above. To construct a homology model of HR1Y+8, residues 183–202 of the HR1 region from 8UTF were used as a template override to model the C-terminal extension absent from 8XO8. For modeling of **17**, residues 449–458 of the HR2 region from 8UTF were used as a template override.

Author contributions

Kazuya Kobayashi: investigation, visualization, writing – original draft. Yuki Yamagushi: investigation. Mizuki Itahara: investigation. Kazushige Hirata: investigation. Keisuke Aoki: investigation, writing – review & editing. Naoya Iwamoto: investigation, writing – review & editing. Hironori Hayashi: formal analysis, investigation, writing – review & editing. Eiichi Kodama: conceptualization, data curation, funding acquisition, methodology, project administration, supervision, writing – review & editing. Shinya Oishi: conceptualization, data curation, funding acquisition, methodology, project administration, supervision, writing – review & editing.

Conflicts of interest

The authors declare that they have no known competing financial interests or personal relationships that could have appeared to influence the work reported in this paper.

Data availability

The data supporting this article have been included as part of the supplementary information (SI). See DOI: https://doi.org/10.1039/d6md00211k.

Supplementary information: the SI includes analytical characterization (ESI-MS, HPLC) of synthesized peptides, supplementary biological assay data, CD analysis, and molecular models.

Acknowledgements

This work was supported by JSPS KAKENHI, Japan (JP16H05346; JP19H03701; JP21K19366); Research on Development of New Drugs (JP20ak0101140) from AMED, Japan. We would like to acknowledge the technical support given by the Biomedical Research Core of the Tohoku University Graduate School of Medicine, Disaster Resilience Co-creation Center and Core-Research Cluster of Disaster Science (IRIDeS, Tohoku University).

References

1 B. Rima, A. Balkema-Buschmann, W. G. Dundon, P. Duprex, A. Easton, R. Fouchier, G. Kurath, R. Lamb, B. Lee, P. Rota and L. Wang, Paramyxoviridae, *J. Gen. Virol.*, 2019, **100**, 1593–1594.

2 J. M. Hübschen, I. Gouandjika-Vasilache and J. Dina, *Lancet*, 2022, **399**, 678–690.

3 A. Misin, R. M. Antonello, S. Di Bella, G. Campisciano, N. Zanotta, D. R. Giacobbe, M. Comar and R. Luzzati, *Microorganisms*, 2020, **8**, 276.

4 D. E. Griffin, *Viral Immunol.*, 2018, **31**, 86–95.

5 R. Huits, D. Buonfrate, K. O'Laughlin, D. H. Hamer and M. Libman, *Travel Med. Infect. Dis.*, 2025, **67**, 102885.

6 R. K. Garg, A. Mahadevan, H. S. Malhotra, I. Rizvi, N. Kumar and R. Uniyal, *Rev. Med. Virol.*, 2019, **29**, e2058.

7 P. Plattet, L. Alves, M. Herren and H. C. Aguilar, *Viruses*, 2016, **8**, 112.

8 C. K. Navaratnarajah, A. R. Generous, I. Yousaf and R. Cattaneo, *J. Biol. Chem.*, 2020, **295**, 2771–2786.

9 M. A. Brindley, P. Plattet and R. K. Plemper, *Proc. Natl. Acad. Sci. U. S. A.*, 2014, **111**, E3795–E3804.

10 B. Berkhout, D. Eggink and R. W. Sanders, *Curr. Opin. Virol.*, 2012, **2**, 50–59.

11 S. Xia, L. Yan, W. Xu, A. S. Agrawal, A. Algaissi, C. T. K. Tseng, Q. Wang, L. Du, W. Tan, I. A. Wilson, S. Jiang, B. Yang and L. Lu, *Sci. Adv.*, 2019, **5**, eaav4580.

12 V. K. Outlaw, S. Bottom-Tanzer, D. F. Kreitler, S. H. Gellman, M. Porotto and A. Moscona, *J. Am. Chem. Soc.*, 2019, **141**, 12648–12656.

13 D. M. Lambert, S. Barney, A. L. Lambert, K. Guthrie, R. Medinas, D. E. Davis, T. Bucy, J. Erickson, G. Merutka and S. R. Petteway, *Proc. Natl. Acad. Sci. U. S. A.*, 1996, **93**, 2186–2191.

14 J. C. Welsch, A. Talekar, C. Mathieu, A. Pessi, A. Moscona, B. Horvat and M. Porotto, *J. Virol.*, 2013, **87**, 13785–13794.

15 M. Watanabe, K. Hashimoto, Y. Abe, E. N. Kodama, R. Nabika, S. Oishi, S. Ohara, M. Sato, Y. Kawasaki, N. Fujii and M. Hosoya, *PLoS One*, 2016, **11**, e0162823.

16 T. N. Figueira, L. M. Palermo, A. S. Veiga, D. Huey, C. A. Alabi, N. C. Santos, J. C. Welsch, C. Mathieu, B. Horvat, S. Niewiesk, A. Moscona, M. A. R. B. Castanho and M. Porotto, *J. Virol.*, 2017, **91**, e01554-16.

17 F. T. Bovier, K. Rybkina, S. Biswas, O. Harder, T. C. Marcink, S. Niewiesk, A. Moscona, C. A. Alabi and M. Porotto, *ACS Nano*, 2021, **15**, 12794–12803.

18 D. R. Kelsey, T. D. Flanagan, J. Young and P. L. Yeagle, *J. Biol. Chem.*, 1990, **255**, 12178–12183.

19 E. Malvoisin and F. Wild, *J. Viol.*, 1990, **64**, 5160–5162.

20 T. Hashiguchi, Y. Fukuda, R. Matsuoka, D. Kuroda, M. Kubota, Y. Shirogane, S. Watanabe, K. Tsumoto, D. Kohda, R. K. Plemper and Y. Yanagi, *Proc. Natl. Acad. Sci. U. S. A.*, 2018, **115**, 2496–2501.

21 D. S. Zyla, R. D. Marca, G. Niemeyer, G. Zipursky, K. Stearns, C. Leedale, E. B. Sobolik, H. M. Callaway, C. Hariharan, W. Peng, D. Parekh, T. C. Marcink, R. D. Avalos, B. Horvat, C. Mathieu, J. Snijder, A. L. Greninger, K. M. Hastie, S. Niewiesk, A. Moscona, M. Porotto and E. O. Saphire, *Science*, 2024, **384**, eadm8693.

22 A. Otaka, M. Nakamura, D. Nameki, E. Kodama, S. Uchiyama, S. Nakamura, H. Nakano, H. Tamamura, Y. Kobayashi, M. Matsuoka and N. Fujii, *Angew. Chem., Int. Ed.*, 2002, **41**, 2937–2940.

23 S. Oishi, S. Ito, H. Nishikawa, K. Watanabe, M. Tanaka, H. Ohno, K. Izumi, Y. Sakagami, E. Kodama, M. Matsuoka and N. Fujii, *J. Med. Chem.*, 2008, **51**, 388–391.

24 H. Nishikawa, S. Oishi, M. Fujita, K. Watanabe, R. Tokiwa, H. Ohno, E. Kodama, K. Izumi, K. Kajiwara, T. Naitoh, M. Matsuoka, A. Otaka and N. Fujii, *Bioorg. Med. Chem.*, 2008, **16**, 9184–9187.

25 A. Takahara, T. Nakatsu, K. Hirata, H. Hayashi, K. Kawaji, K. Aoki, S. Inuki, H. Ohno, H. Kato, E. Kodama and S. Oishi, *J. Med. Chem.*, 2025, **68**, 3123–3133.

26 K. Hirata, A. Takahara, S. Suzuki, S. Murakami, K. Kawaji, A. Nishiyama, M. Sasano, M. Shoji-Ueno, E. Usui, K. Murayama, H. Hayashi, S. Oishi and E. N. Kodama, *iScience*, 2024, **27**, 108961.

27 J. Zhu, C. W. Zhang, Y. Qi, P. Tien and G. F. Gao, *Biochem. Biophys. Res. Commun.*, 2002, **299**, 897–902.

28 K. Izumi, E. Kodama, K. Shimura, Y. Sakagami, K. Watanabe, S. Ito, T. Watabe, Y. Terakawa, H. Nishikawa, S. G. Sarafianos, K. Kitaura, S. Oishi, N. Fujii and M. Matsuoka, *J. Biol. Chem.*, 2009, **284**, 4914–4920.

29 T. Watabe, Y. Terakawa, K. Watanabe, H. Ohno, H. Nakano, T. Nakatsu, H. Kato, K. Izumi, E. Kodama, M. Matsuoka, K. Kitaura, S. Oishi and N. Fujii, *J. Mol. Biol.*, 2009, **392**, 657–665.

30 S. Liu, H. Lu. J. Niu, Y. Xu, S. Wu and S. Jiang, *J. Biol. Chem.*, 2005, **280**, 11259–11273.
31 K. Champagne, A. Shishido and M. J. Root, *J. Biol. Chem.*, 2009, **284**, 3619–3627.
32 W. Bi, G. Chen and B. Dang, *J. Virol.*, 2022, **96**, e0068122.
33 K. Hashimoto, H. Maeda, K. Miyazaki, M. Watanabe, S. Norito, R. Maeda, Y. Kume, T. Ono, M. Chishiki, K. Suyama, M. Sato and M. Hosoya, *Jpn. J. Infect. Dis.*, 2021, **74**, 154–156.